

## Article

# Investigation of the Positive Temperature Coefficient Resistivity of Nb-Doped Ba<sub>0.55</sub>Sr<sub>0.45</sub>TiO<sub>3</sub> Ceramics

Yifei Wang and Xiaoyang Chen \*

College of Materials Science and Engineering, Sichuan University, Chengdu 610064, China;  
2021223010009@stu.scu.edu.cn

\* Correspondence: xiaoyang189@scu.edu.cn

**Abstract:** The demands of low-Curie-temperature ( $\sim -10$  °C) positive temperature coefficient (PTC) thermistors are increasing in advanced precision integrated circuits and other industries. In this paper, the Nb-doped Ba<sub>0.55</sub>Sr<sub>0.45</sub>TiO<sub>3</sub>(BST)-based PTC resistivity materials are reported. The effects of the sintering process, especially the cooling rate on the PTC properties of the material, are investigated. The results indicate that the Ba<sub>0.55</sub>Sr<sub>0.45</sub>Ti<sub>0.9985</sub>Nb<sub>0.0015</sub>O<sub>3</sub> composition of the prepared PTC ceramics demonstrates promising PTC characteristics. These include a Curie temperature as low as  $-13$  °C, a high temperature coefficient of 0.296 at  $-3.4$  °C, a large enough resistivity change of 3.1 over a narrow phase transition temperature range of approximately 38 °C, and moderate resistivity below the Curie temperature. Such properties suggest that the Ba<sub>0.55</sub>Sr<sub>0.45</sub>Ti<sub>0.9985</sub>Nb<sub>0.0015</sub>O<sub>3</sub> ceramics are likely suitable for use in thermal management systems designed for low-temperature control.

**Keywords:** Ba<sub>1-x</sub>Sr<sub>x</sub>TiO<sub>3</sub>; Curie temperature point; phase transition; PTC; ceramic



Citation: Wang, Y.; Chen, X.

Investigation of the Positive Temperature Coefficient Resistivity of Nb-Doped Ba<sub>0.55</sub>Sr<sub>0.45</sub>TiO<sub>3</sub> Ceramics. *Crystals* **2024**, *14*, 419. <https://doi.org/10.3390/cryst14050419>

Academic Editor: Maria Gazda

Received: 19 April 2024

Revised: 28 April 2024

Accepted: 28 April 2024

Published: 29 April 2024



**Copyright:** © 2024 by the authors. Licensee MDPI, Basel, Switzerland. This article is an open access article distributed under the terms and conditions of the Creative Commons Attribution (CC BY) license (<https://creativecommons.org/licenses/by/4.0/>).

## 1. Introduction

Materials that exhibit a positive temperature coefficient (PTC) of resistivity are commonly used in applications such as thermistors, temperature-regulated heaters, and thermostat components. Their resistivity can increase dramatically, often by several orders of magnitude, either at a specific temperature or within a particular temperature range, attributed to the material's phase transition. In practical applications, this specific temperature or temperature range is often referred to as the switch temperature, because the PTC component functions as a temperature switch.

Up to now, most of the reported PTC resistivity materials focus on applications in which the switch temperatures are higher than room temperature ( $>50$  °C, normally). However, the demands for temperature control at low temperatures have been increasing. For instance, it is well known that the performance degradation of Li-ion batteries is a great challenge for electric vehicles in winter and low-temperature environments ( $<10$  °C) [1,2]. Various thermal preheating and management systems for Li-ion batteries are proposed to support the batteries' functionality in low-temperature environment [3–6]. In the above systems, proper PTC thermistors ( $T_c \sim -10$  °C) are required to manage the work of heaters. In addition, PTC thermistors with low switch temperatures ( $\sim -10$  °C) are also demanded in aerospace and precision integrated circuits and other industries.

Currently, PTC resistivity materials with low switch temperatures, especially lower than  $-0$  °C, have been paid increasing attention. As a traditional inorganic PTC ceramic, BaTiO<sub>3</sub> (BT) has a large PTC intensity. The PTC effect of BT ceramics arises from the phase transition from the ferroelectric phase to paraelectric phase. When the temperature exceeds the Curie temperature of the BT ceramics, the phase structures will change from ferroelectric into paraelectric and their resistivities will show exponential growth around  $T_c$ . The  $T_c$  of pure BT ceramics is around 120 °C. Its  $T_c$  could be modulated to higher or lower temperatures by proper element doping. So far, the switch temperatures of BT-based PTC ceramics are almost higher than 50 °C. Even though the Curie temperature

could be shifted to a lower temperature ( $<0\text{ }^{\circ}\text{C}$ ) by heavy doping on the A-site or B-site [7,8], there are few reports of BT-based PTC materials with a low temperature ( $<0\text{ }^{\circ}\text{C}$ ). A significant challenge is that heavy doping often results in an inhomogeneous composition, which can cause a relaxation phase transition that would weaken the PTC performance of BT-based PTC ceramics, such as reduced PTC intensity, and a wide phase transition temperature span [9–11]. For instance, when the Curie temperature moves to below  $25\text{ }^{\circ}\text{C}$ , the temperature range of the phase transition,  $\Delta T$ , tends to widen, and there is a significant reduction in the magnitude of the resistivity jump.

The previous work indicates that the resistivity anomaly increase is related to the barrier layer of the BT ceramic grain boundary. Hasegawa et al. [12–14] reported that the PTC performance of BT ceramics could be enhanced by increasing the height of the ceramic grain boundary barrier  $\varphi_0$ , and the height of the barrier  $\varphi_0$  is directly proportional to the square of the interface state density at the grain boundary of BT ceramics [12]. According to the above knowledge, one of the possible approaches could be to increase the adsorbed oxygen on the grain boundaries by the proper reoxidation process or proper elements dropping combined with the proper sintering process in which the adsorbed oxygen would be increased on the grain boundaries and form the interface states.

The Nb-doped  $\text{BaTiO}_3$  ceramics were demonstrated to show a pronounced PTC effect [15–17]. In this work, Nb-doped  $\text{Ba}_{0.55}\text{Sr}_{0.45}\text{TiO}_3$  (BST) and  $\text{Ba}_{0.55}\text{Sr}_{0.45}\text{Ti}_{(1-x)}\text{Nb}_x\text{O}_3$  ceramics were fabricated and the PTC properties of the prepared ceramics were investigated. Different ceramic sintering processes with five different cooling rates were investigated to promote the PTC performance. The influence of the cooling rate on the ceramic grain boundary barrier  $\varphi_0$  and interface states of the grain boundary were analyzed, respectively.

## 2. Materials and Methods

Ceramic powders composed of  $\text{Ba}_{0.55}\text{Sr}_{0.45}\text{Ti}_{(1-x)}\text{Nb}_x\text{O}_3$  ( $x = 0.001, 0.0015, 0.002, 0.0025, 0.003$ ) were synthesized using the sol-gel method. The precursor materials  $\text{Ba}(\text{CH}_3\text{COOH})_2$  (Aladdin, Shanghai, China, 99%),  $\text{Sr}(\text{CH}_3\text{COOH})_2$  (Aladdin, Shanghai, China, 99%),  $\text{Ti}(\text{OC}_4\text{H}_9)_4$  (Chron, Chengdu, China, 98.5%), and  $\text{Nb}(\text{OC}_2\text{H}_5)_5$  (Acmech, Shanghai, China, 99%), were weighed to match the intended stoichiometric proportions. As solvents in the process, diethanol methyl ether, ethanol acetic acid, and deionized water were utilized. First,  $\text{Ba}(\text{CH}_3\text{COO})_2$  and  $\text{Sr}(\text{CH}_3\text{COO})_2$  were dissolved in water. Second,  $\text{Ti}(\text{OC}_4\text{H}_9)_4$  and  $\text{Nb}(\text{OC}_2\text{H}_5)_5$  were then dissolved in a mixture of ethanol and acetic acid with a volume ratio of 1:1. The two sets of solutions were blended and stirred for 60 min until a clear and transparent sol formed at  $60\text{ }^{\circ}\text{C}$ . This solution gradually transitioned into a gel. The gel was then air-dried at  $80\text{ }^{\circ}\text{C}$ . The resulting xerogel underwent carbonization at  $350\text{ }^{\circ}\text{C}$  and was calcined at  $950\text{ }^{\circ}\text{C}$  for 3 h in air. The resulting fine powder was then granulated and compressed into discs measuring 1.0 cm in diameter and 1.0 mm in thickness at a pressure of 10 MPa, using polyvinyl alcohol (PVA) as a binder. These discs were subsequently calcined at  $550\text{ }^{\circ}\text{C}$  to remove the PVA binder. Following this, the pellets were sintered at  $1400\text{ }^{\circ}\text{C}$  in the air for 3 h and then quenched to room temperature. To explore the effect of the cooling rate, the specimen with the composition of  $\text{Ba}_{0.55}\text{Sr}_{0.45}\text{Ti}_{0.9985}\text{Nb}_{0.0015}\text{O}_3$  was sintered in air at  $1400\text{ }^{\circ}\text{C}$  for 3 h and then cooled to  $900\text{ }^{\circ}\text{C}$  with cooling rates of  $250\text{ }^{\circ}\text{C}/\text{h}$ ,  $210\text{ }^{\circ}\text{C}/\text{h}$ ,  $180\text{ }^{\circ}\text{C}/\text{h}$ ,  $150\text{ }^{\circ}\text{C}/\text{h}$ , and  $90\text{ }^{\circ}\text{C}/\text{h}$ , respectively.

The phase structure of the specimens was examined using X-ray diffraction (DX-2700, Dandong, China) with  $\text{Cu K}\alpha$  radiation. This analysis was conducted at 40 kV and 30 mA, using a step size of 0.02 and a duration of 1 s per step. Additionally, the microscopic morphology of the specimens was investigated through a Cold Field Emission Scanning Electron Microscope (JSM-7500F, Tokyo, Japan).

The resistance-temperature ( $R$ - $T$ ) characteristics of the ceramic specimens were evaluated from  $-40$  to  $100\text{ }^{\circ}\text{C}$  using an Electrometer (Keithley 6517B, Cleveland, OH, USA) at an operating voltage of 2 V, within a temperature-controlled chamber equipped with a programmable controller. The  $R$ - $T$  performance was assessed through continuous heating and cooling cycles.

The temperature characteristics of the capacitors were measured using LCR meters (Tonghui TH2827C, Changzhou, China). The capacitance temperature tests were conducted at a frequency of 100 kHz, within a temperature span of  $-60$  to  $120$  °C. For impedance data, the tests were carried out at a voltage of 2 V, across a frequency range from 20 Hz to 1 MHz.

### 3. Results and Discussion

#### 3.1. The Temperature Dependence of the Electrical Resistivity of Nb-Doping BST Ceramics

The resistivity-temperature ( $\rho$ - $T$ ) curves for specimens with varying Nb doping concentrations are displayed in Figure 1a. To clearly assess the resistivity-temperature response,  $\rho_{min}$  is designated as the resistivity at  $-40$  °C, since the resistivities exhibit a monotonic increase before the phase transition within the examined temperature range, as illustrated in Figure 1a. Additionally, the Curie temperature  $T_c$  of the ceramics is established by analyzing the dielectric constant-temperature curves presented in the Figure 1b inset. The temperature coefficient of resistivity ( $\alpha_T$ ) was calculated as follows:

$$\alpha_T = \frac{1}{R_T} \frac{dR_T}{dT} \times 100\% \quad (1)$$

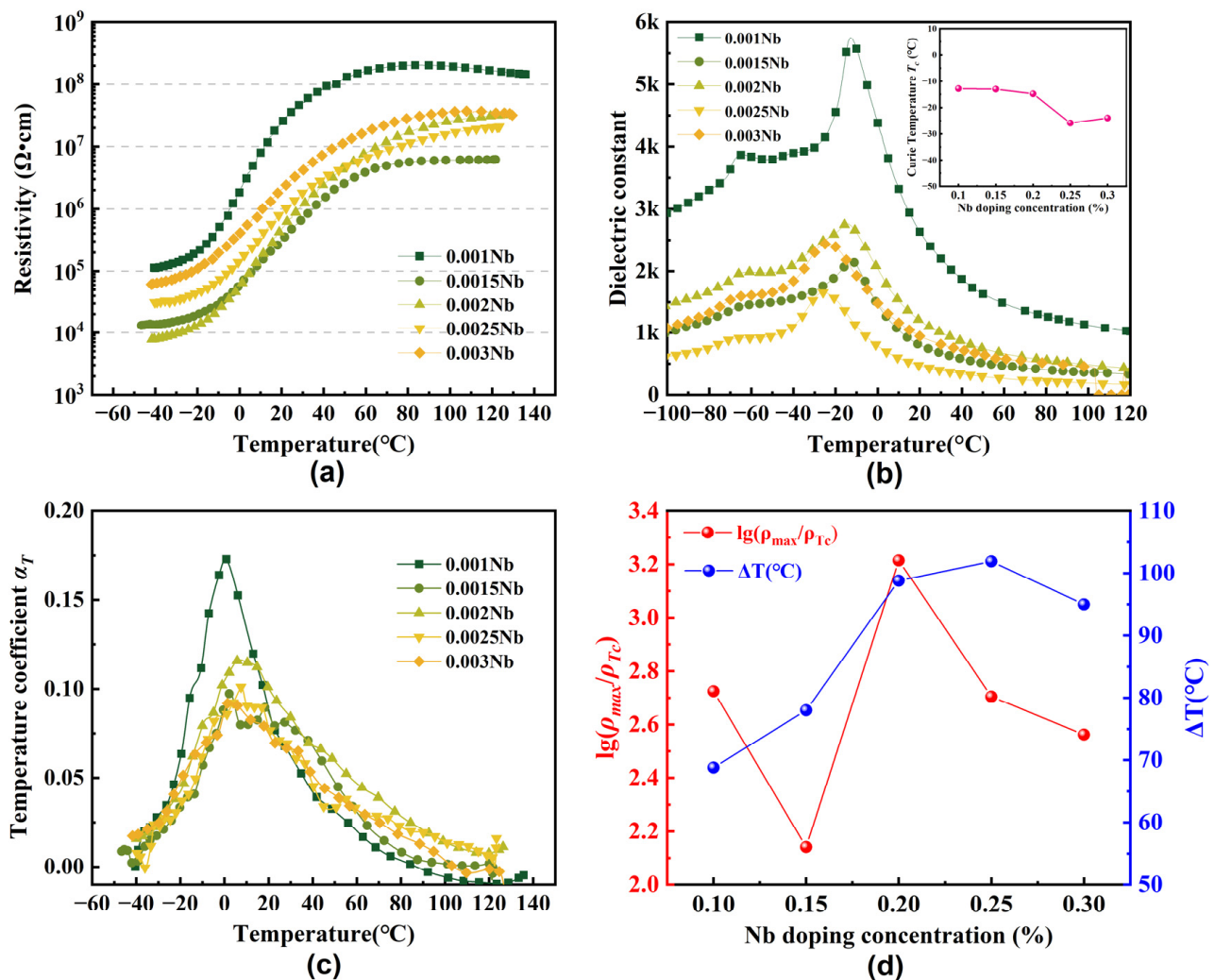


**Figure 1.** (a) The  $\rho$ - $T$  curves of the specimens with varying Nb concentrations, (b) the Curie Temperature  $T_c$  vs. Nb concentration at different temperatures, (c) the  $\alpha_T$ - $T$  curves of the specimens with varying Nb concentrations at different temperatures, (d) the  $\lg(\rho_{max}/\rho_{Tc})$  and  $\Delta T$  curves vs. the Nb concentration, respectively.

$R_T$  means the resistivity corresponding to the temperature  $T$ . The resistivity jumping of the ceramics is defined as  $\lg(\rho_{max}/\rho_{Tc})$ . The maximum resistivity  $\rho_{max}$  is defined as the resistivity values that  $\alpha_T$  values drop to 0.025 after phase transition. As shown in Figure 1a, the resistivities increase monotonically even after the phase transition, except the one with  $x = 0.001$  in our case. The temperature range of the phase transition, denoted as  $\Delta T$ , is defined as  $\Delta T = T_{\rho_{max}} - T_c$ . A narrow  $\Delta T$  means a rapid phase transition.

The curves in Figure 1a show that all the ceramics with different Nb content possess an obvious PTC effect, and the resistivity jumps are around two to three orders of magnitude for all specimens. There is a mild negative temperature coefficient phenomenon that appeared after the phase transition in the tested temperature range for the specimens with  $x = 0.001$ , attributed to a decrease in the barrier height [14]. For the specimen with  $x = 0.0015$ , a nearly flat plateau is noted in the temperature range from 40 °C to 130 °C. For the other specimens, the resistivities show a slight increase with the increase in temperature from 40 °C to 130 °C. In the region of the Nb<sup>5+</sup> doping concentration, the  $\rho_{min}$  shows the smallest value of  $7.2 \times 10^3 \Omega \cdot \text{cm}$  at an Nb content of 0.002. For the other ceramics, the  $\rho_{min}$  values are approximately  $10^4 \Omega \cdot \text{cm}$ .

The fluctuation of  $T_c$  with the Nb<sup>5+</sup> concentration is shown in the Figure 1b inset. The  $T_c$  of the specimens with  $x = 0.001$ , 0.0015, and 0.002 are  $-12.8$  °C,  $-13.1$  °C, and  $-14.3$  °C, respectively. With the further increase in the Nb<sup>5+</sup> concentration, the  $T_c$  reduced to lower than  $-20$  °C. Figure 1c shows the temperature dependences of the temperature coefficient of resistivity  $\alpha_T$  of the specimens. Among them, the specimens with  $x = 0.001$  give the highest value of  $\sim 17.5\%$ , and the  $\alpha_T$  decreases with the increase in the doping Nb<sup>5+</sup> concentration. Because the dielectric constant -temperature peaks tend to widen with the increase in the Nb<sup>5+</sup> concentration (see Figure 1b), the results reveal that the phase transition of Ba<sub>0.55</sub>Sr<sub>0.45</sub>Ti<sub>(1-x)</sub>Nb<sub>x</sub>O<sub>3</sub> ceramics tends to be relaxed due to the increasing Nb<sup>5+</sup> entering into the BST lattice. The broadening of the phase transition temperature range is a result of the relaxation phase transition. Additionally, a notable broader  $\Delta T$  when the Nb<sup>5+</sup> content exceeds 0.0015 also confirms this (see Figure 1d).

Figure 2 shows the XRD patterns of all specimens. Figure 2a is conducted at 0 °C, and Figure 2b is 20 °C, respectively. Compared with the PDF cards #074-9859 and #005-7689, all the specimens show a pure perovskite phase, and no second phase was detected in the tested range. The diffraction peaks of all the specimens show slight left-shifting with the increase in the Nb<sup>5+</sup> concentration, which indicates the enlarged lattice due to the Nb<sup>5+</sup> entered into the BST lattice. Clear asymmetrical (200) peaks can be observed at around 46 degrees in Figure 2a,b. These peaks' shapes can be fitted as the overlapping of the cubic (200) peaks and the tetragonal (002) and (200) peaks (see Figure 2c). The results suggest that the specimens were undergoing the phase transition from the tetragonal to the cubic phase at the temperatures. The phase compositions of the specimens were calculated by the RIR method according to the XRD data (see Figure 2d). The results show that the tetragonal phase was still the main phase component at 0 °C for all the specimens, even though the phase transition started at a  $T_c$  far below 0 °C. As the temperature rose to 20 °C, the situation changed. The main phase component turned to be a cubic phase, especially for the specimens with 0.001, 0.0015, and 0.002 Nb<sup>5+</sup> contents. Anyway, the phase transition is not finished at this stage. The results are consistent with the results in Figure 1a.

Given that smaller values of both  $\rho_{min}$  and  $\Delta T$  are desirable for practical applications, it is important to note that a smaller  $\rho_{min}$  lowers the power consumption of PTC thermistors, while a narrower  $\Delta T$  enhances the temperature control. The specimen with 0.0015 Nb<sup>5+</sup> content was chosen for further exploration, as it showed both low resistivity ( $1.4 \times 10^4 \Omega \cdot \text{cm}$ ) and a narrow temperature span ( $\sim 78$  °C) comprehensively. The possibility of improving the PTC performance of the Ba<sub>0.55</sub>Sr<sub>0.45</sub>Ti<sub>0.9985</sub>Nb<sub>0.0015</sub>O<sub>3</sub> ceramics by optimizing the cooling rate of the ceramic sintering process is explored in this work.

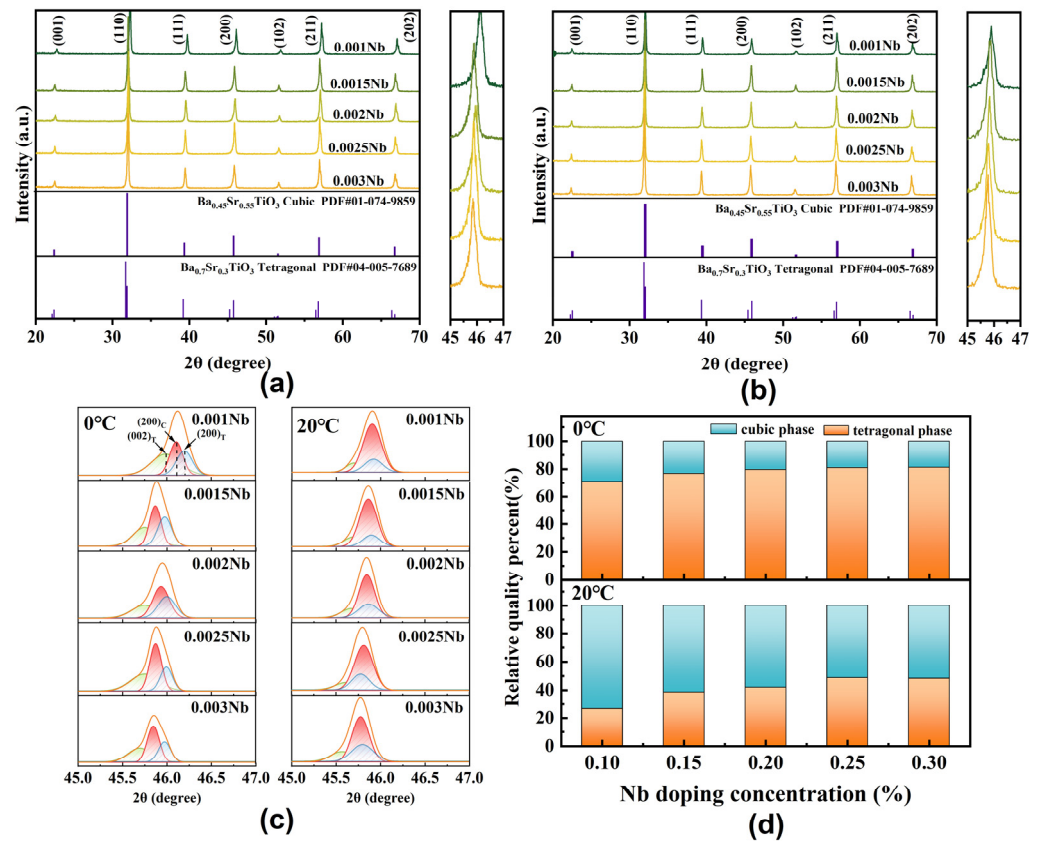


**Figure 2.** XRD patterns of the prepared  $\text{Ba}_{0.55}\text{Sr}_{0.45}\text{Ti}_{(1-x)}\text{Nb}_x\text{O}_3$  ceramics: (a) 0 °C and (b) 20 °C. (c) A close observation in  $2\theta$  ranging from 45° to 47°. (d) Calculated relative quality percentages of tetragonal and cubic phases at 0 °C and 20 °C.

### 3.2. Influences of the Cooling Rate on Nb-BST Ceramics

Previous research demonstrates that the PTC properties of  $\text{BaTiO}_3$  ceramics are highly sensitive to the specimens' microstructure and defect chemistry. These factors are in turn greatly influenced by the processing parameters like the sintering condition [18,19] and heat treatment [20,21], etc. The  $\text{Ba}_{0.55}\text{Sr}_{0.45}\text{Ti}_{0.9985}\text{Nb}_{0.0015}\text{O}_3$  ceramics were sintered by different cooling rates, and the influence of the cooling rate on the microstructure and the PTC properties were investigated.

Figure 3a shows the  $\rho$ - $T$  curves of the  $\text{Ba}_{0.55}\text{Sr}_{0.45}\text{Ti}_{0.9985}\text{Nb}_{0.0015}\text{O}_3$  ceramic specimens with different cooling rates. Compared with the specimen quenched, the PTC intensities of the others were enhanced significantly. Some of the resistivity jumps exceed three orders of magnitude. All the curves show almost plateau shapes after the phase transition. Within the entire testing temperature range, the resistivity and the temperature are positively correlated. Figure 3b shows the influence of the cooling rates on  $\rho_{min}$  and  $\rho_{max}$ . Both the  $\rho_{min}$  and  $\rho_{max}$  values increased with a decrease in the cooling rate. They show different changing characteristics. The  $\rho_{min}$  values increased slightly from  $1.4 \times 10^4 \Omega \cdot \text{cm}$  to  $1.8 \times 10^4 \Omega \cdot \text{cm}$  when the cooling rate was higher than 180 °C/h and then increased sharply with the decrease in the cooling rate, while the  $\rho_{max}$  values increased sharply at first from  $5.9 \times 10^6 \Omega \cdot \text{cm}$  to  $1.6 \times 10^8 \Omega \cdot \text{cm}$  when the cooling rate reduced to 210 °C/h from 250 °C/h and tended to become milder at the cooling rates of 210 °C/h, 180 °C/h, and 150 °C/h and then increase largely at 90 °C/h. The results indicate that the specimens with cooling rates of 180 °C/h and 210 °C/h could produce a large resistivity jump during the phase transition. The fluctuation of the temperature coefficient  $\alpha_T$  with temperature is shown in Figure 3c. Compared with the quenched specimen, all  $\alpha_T$  values of the specimens with different cooling rates were improved. Among them, the specimen with the cooling rate of 180 °C/h shows the largest increase, from 0.10 to 0.296, and the sharpest  $\alpha$  vs.  $T$

curve, which reveals the narrowest phase transition temperature span. Figure 3d gives the cooling rate dependence of  $\lg(\rho_{max}/\rho_{T_c})$  and  $\Delta T$ . The magnitude of the resistivity change is higher than 3 for specimens with a cooling rate of 210 °C/h to 180 °C/h, reaching 3.3 and 3.1, respectively. The values of  $\Delta T$  reduced significantly with the decrease in the cooling rate. Among them, the specimen with a 180 °C/h cooling rate shows the smallest value,  $\sim 38$  °C.

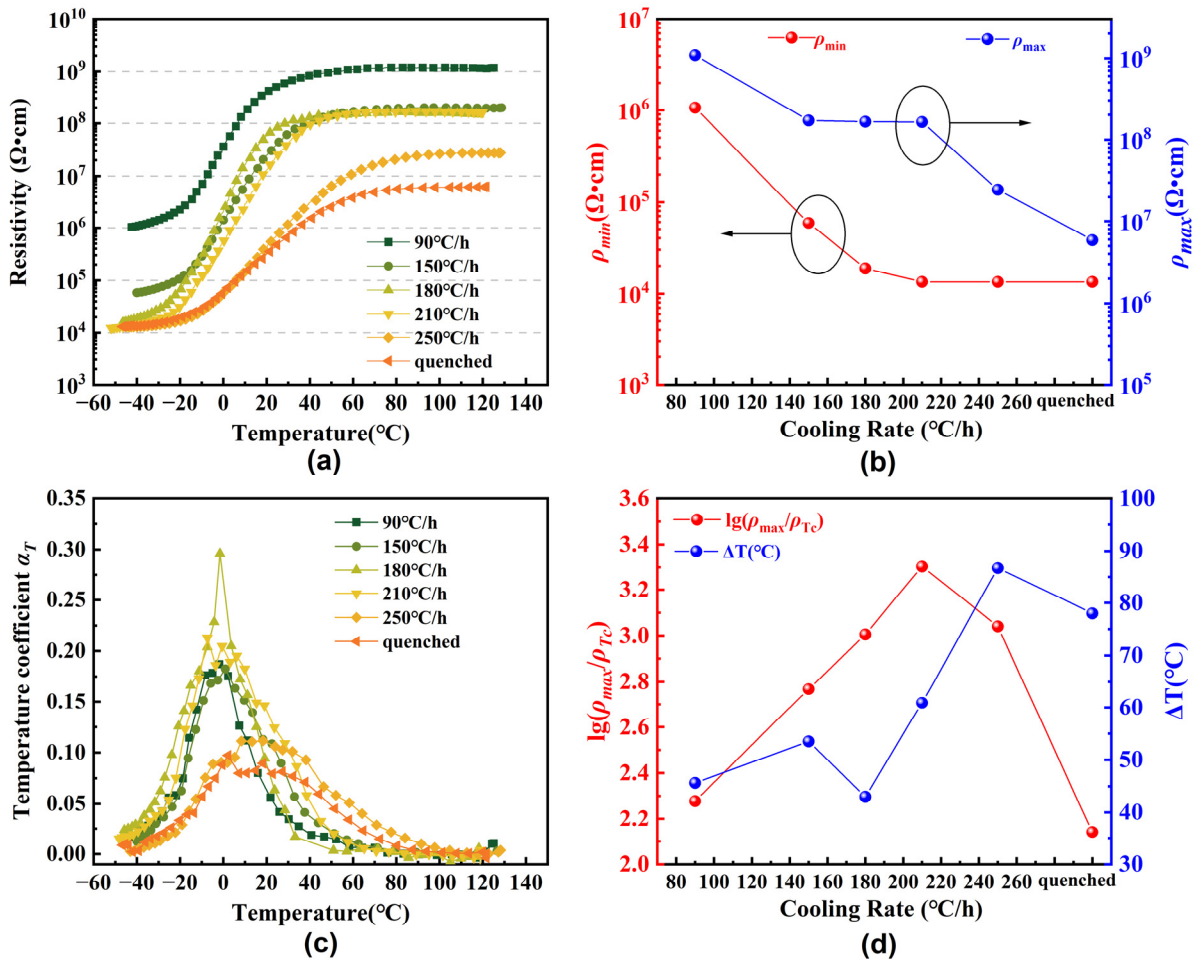


**Figure 3.** The (a)  $\rho$ - $T$  curves of specimens with different cooling rates, (b) the resistivities of specimens with different cooling rates at different temperatures, (c)  $\alpha_T$  vs. cooling rates at different temperatures, (d)  $\lg(\rho_{max}/\rho_{T_c})$  and  $\Delta T$  vs. cooling rates.

Figure 4 illustrates the XRD patterns of the specimens with different cooling rates. The tests were carried out at around 0 °C and 20 °C, respectively. Compared with the results of Figure 2, no second phase was detected. Similar asymmetrical (200) peaks can also be observed at around 46 degrees in Figure 4a,b, which indicates the coexistence of the cubic phase and tetragonal phase in the specimens. The phase compositions at 0 °C and 20 °C were determined using RIR methods, based on the XRD data presented in Figure 4a,b. As shown in Figure 4d, different from the results in Figure 2d, the results reveal that the main phase component turned to be the cubic phase for all specimens, and the transition from the ferroelectric to the paraelectric phase is almost complete at 20 °C for those specimens with the cooling rates of 90 °C/h, 150 °C/h, and 180 °C/h. The results are consistent with the results in Figure 3a.

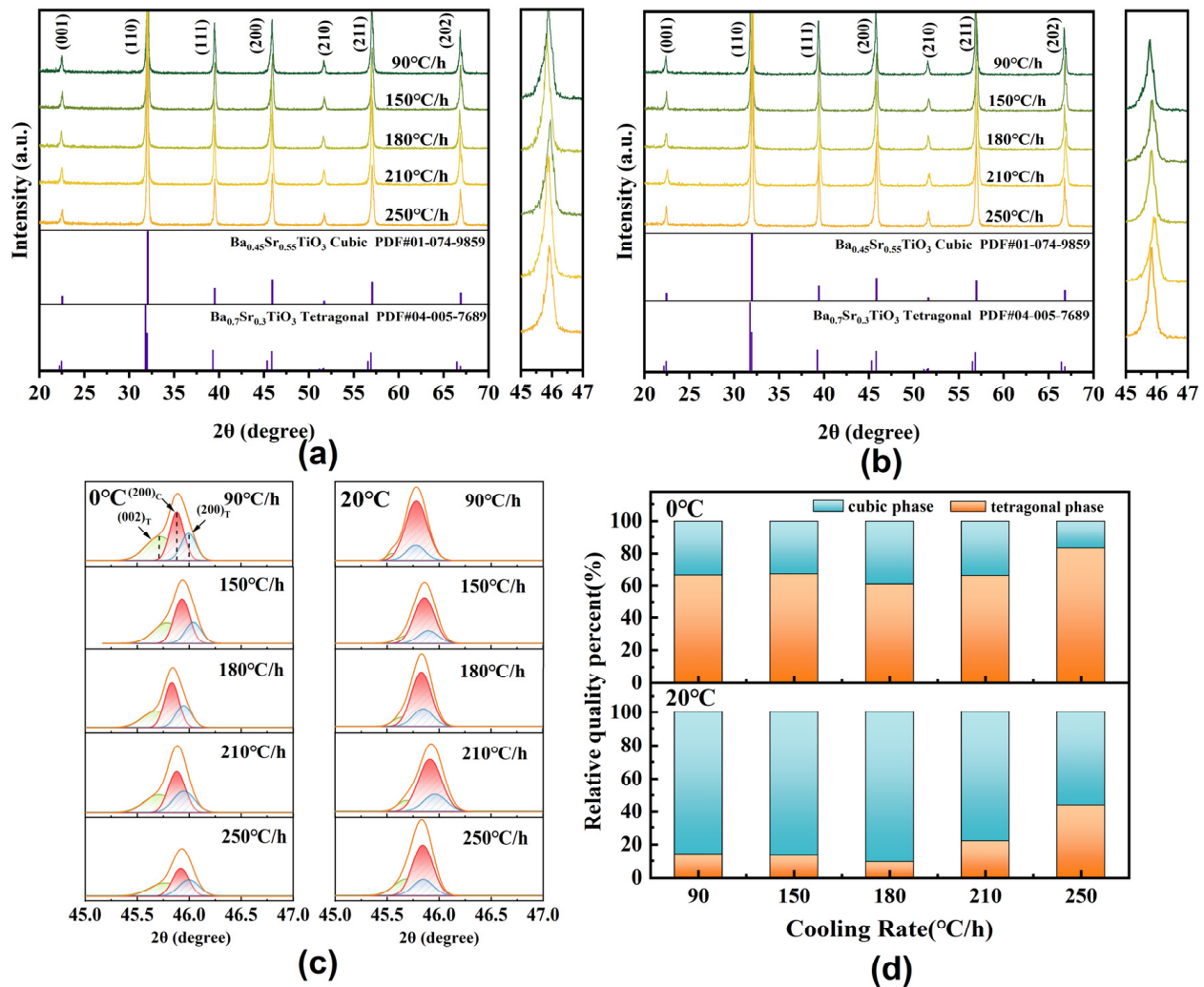


**Figure 4.** XRD patterns of  $\text{Ba}_{0.55}\text{Sr}_{0.45}\text{Ti}_{0.0085}\text{Nb}_{0.0015}\text{O}_3$  ceramic specimens with different cooling rates: (a)  $0^\circ\text{C}$  and (b)  $20^\circ\text{C}$ . (c) A close observation in  $2\theta$  ranging from  $45^\circ$  to  $47^\circ$ . (d) Calculated relative quality percentages of tetragonal and cubic phases at  $0^\circ\text{C}$  and  $20^\circ\text{C}$ .

The cooling rate influenced the resistivity and its change during the phased transition significantly; in turn, the PTC properties of the ceramics were enhanced markedly.

The surface morphology of the specimens with different cooling rates is shown in Figure 5. The SEM images indicate that there are little differences in grain morphology, as all the specimens were sintered at the same temperature. The grains are fully developed with sharp polyhedral edges, and the cleavage plane is distinct. The granular structures exhibit similar characteristics across all samples, with approximately 90% of theoretical density, grain sizes of about 2–3  $\mu\text{m}$ , and a consistent size distribution, regardless of the cooling conditions. Figure 5 shows that, in our work, the morphology of the specimens is not significantly affected by variations in the cooling rate. The uniformity in morphology across all samples indicates that changes in electrical properties likely stem from the impact of defect restoration and/or adsorbed oxygen on the grain boundaries in the specimens by different cooling rate sintering processing.

Figure 6a shows the change in the dielectric constant as a function of temperature for all specimens in Figure 3a. The grain boundary barrier  $\varphi_0$  and interface state density  $N_s$  of the specimens in Figure 3a were calculated from the data in Figures 6b and 6c, respectively, and are shown in Figure 6d.

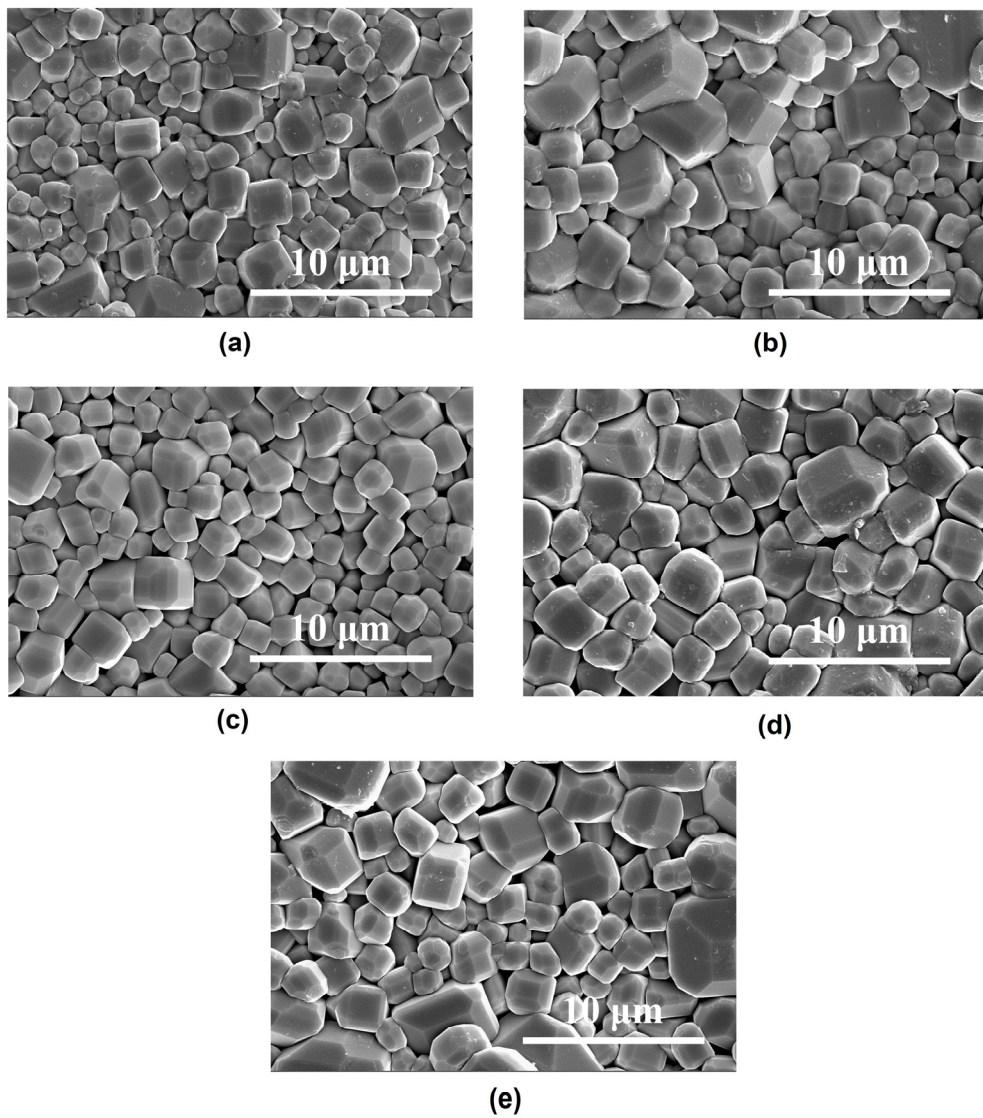


**Figure 5.** SEM images of the Ba<sub>0.55</sub>Sr<sub>0.45</sub>Ti<sub>0.0085</sub>Nb<sub>0.0015</sub>O<sub>3</sub> ceramic specimens with different cooling rates. (a) 250 °C/h; (b) 210 °C/h; (c) 180 °C/h; (d) 150 °C/h; (e) 90 °C/h specimens.

The height of the potential barrier ( $\varphi_0$ ) can be determined using the formula below [22]:

$$\rho_s = \alpha \rho_v \cdot \exp\left(\frac{e\varphi_0}{kT}\right) \quad (2)$$

where  $\rho_s$  is the resistivity of the grain boundary, and  $\rho_v$  means the grain bulk resistivity. The resistivity of ceramics  $\rho = \rho_s + \rho_v$ . When the temperature is much higher than  $T_c$ , the value of  $\rho_s$  will far exceed the value of  $\rho_v$ , so  $\rho \approx \rho_s$  [22]. Then, Equation (2) can be rewritten as

$$\ln \rho_s = \ln(\alpha \rho_v) + e\varphi_0/kT \quad (3)$$

The  $\varphi_0$  can be calculated from the slope of  $\ln \rho_s$  vs.  $1/T$ . The potential barrier  $\varphi_0$  results from a two-dimensional electron trap at the grain boundary, where interface states attract electrons from the bulk and can be expressed as [23]

$$\varphi_0(T > T_c) = \frac{eN_s^2}{8\epsilon_0\epsilon_r N_d} = \frac{eN_s r}{16\epsilon_0\epsilon_a} \quad (4)$$

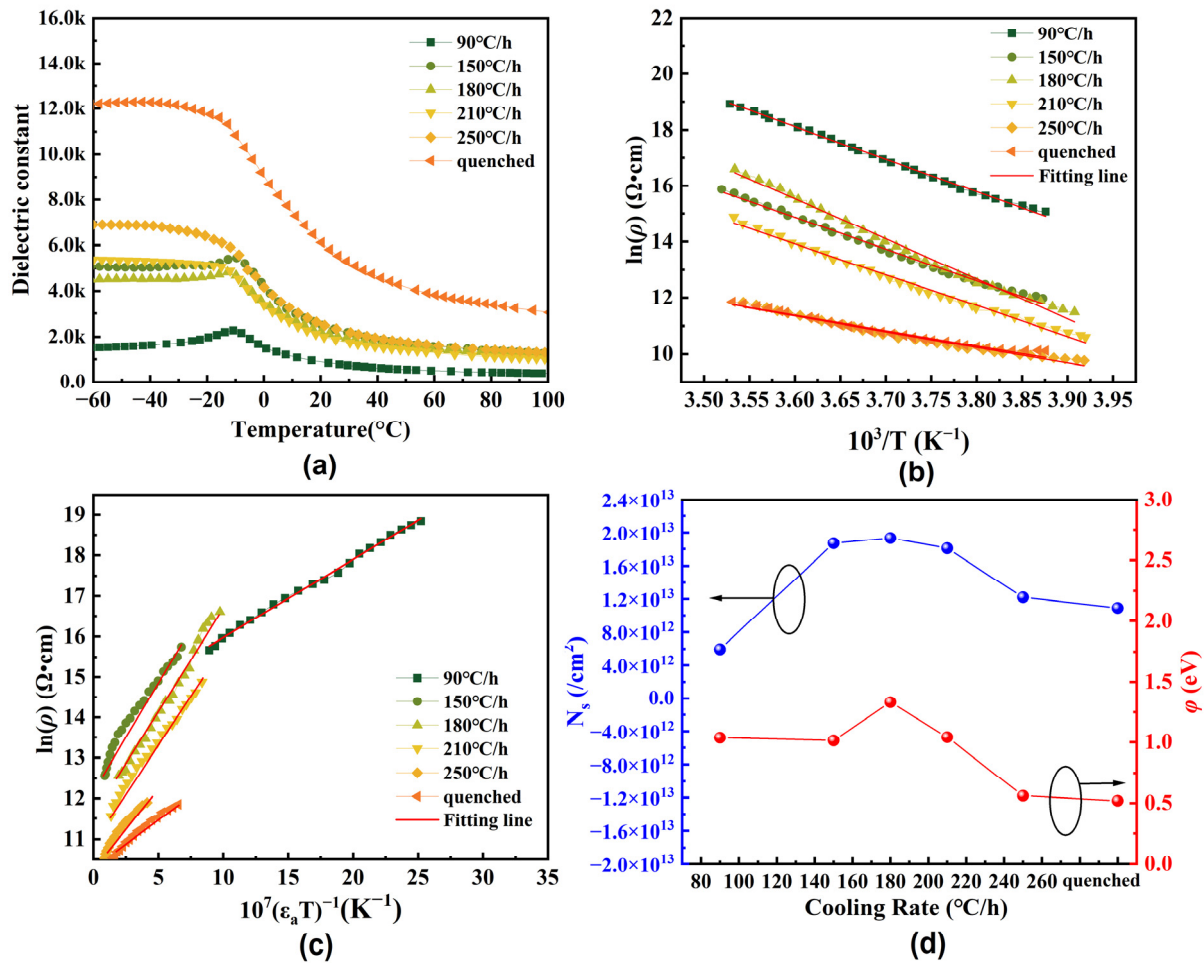


**Figure 6.** (a) Temperature dependence of the dielectric constant of the Ba<sub>0.55</sub>Sr<sub>0.45</sub>Ti<sub>0.0085</sub>Nb<sub>0.0015</sub>O<sub>3</sub> ceramic specimens with different cooling rates. (b) ln(ρ) vs. 10<sup>3</sup>/T and (c) ln(ρ) vs. 10<sup>7</sup>/(ε<sub>a</sub>T) of specimens with different cooling rates. (d) N<sub>s</sub> and φ vs. cooling rates.

Here, N<sub>s</sub> means the ceramic grain boundary interface state density and N<sub>d</sub> is the charged carrier density, ε<sub>0</sub> is the vacuum absolute dielectric constant, ε<sub>r</sub> is the dielectric constant of the grain boundary, e is the constant of elementary charge, r is the grain size, and ε<sub>a</sub> is the apparent dielectric constant. Similarly, Equation (3) can be rewritten as

$$\ln \rho_s = \ln(\alpha \rho_v) + e^2 r N_s / 16 k \epsilon_0 \epsilon_a T \quad (5)$$

It is clear that the value of N<sub>s</sub> is related to the slope of ln(ρ) vs. 1/ε<sub>a</sub>T. Compared with the quenched specimen, the φ<sub>0</sub> and N<sub>s</sub> values of other specimens increased obviously. Among them, the specimens with 180 °C /h and 210 °C /h show a high increase in both φ<sub>0</sub> and N<sub>s</sub>. The results show that the concentration of the interface state density N<sub>s</sub> varies with the cooling rate and the larger interface state density N<sub>s</sub> results in a higher potential barrier.

#### 4. Conclusions

In this work, low-Curie-temperature (<−10 °C) PTCR Ba<sub>0.55</sub>Sr<sub>0.45</sub>Ti<sub>(1-x)</sub>Nb<sub>x</sub>O<sub>3</sub> ceramics were prepared and their PTCR properties were investigated experimentally. Proper Nb doping could cause the T<sub>C</sub> of Ba<sub>0.55</sub>Sr<sub>0.45</sub>TiO<sub>3</sub> ceramics to lower around −10 °C and exhibit a satisfactory PTCR performance. The effect of the cooling rate on the PTC effect of ceramics was investigated. The results indicate that a proper cooling rate would be helpful in increasing the absorption of oxygen located at the grain boundaries during the sintering. The absorbed oxygen at the ceramic boundaries could act as the surface states to increase

the grain boundary potential barrier. As a result, the PTC property of the ceramics could be improved. The  $\text{Ba}_{0.55}\text{Sr}_{0.45}\text{Ti}_{0.9985}\text{Nb}_{0.0015}\text{O}_3$  ceramics with a  $180\text{ }^\circ\text{C}/\text{h}$  cooling rate showed a resistivity jump of 3.1 in a narrow  $\Delta T$  of  $38\text{ }^\circ\text{C}$  and a very high temperature coefficient of 0.296 at  $-3.4\text{ }^\circ\text{C}$ . The  $T_c$  is  $\sim 13\text{ }^\circ\text{C}$ . Compared with the reported low-Curie-temperature PTCR materials [9–11,24,25],  $\text{Ba}_{0.55}\text{Sr}_{0.45}\text{Ti}_{0.9985}\text{Nb}_{0.0015}\text{O}_3$  ceramics exhibit outstanding comprehensive PTCR performance. In particular, the proper  $T_c$  ( $\sim -13\text{ }^\circ\text{C}$ ), the acceptable narrow temperature span ( $\Delta T$ ,  $38\text{ }^\circ\text{C}$ ), and the sufficiently large resistivity jump value ( $\sim 3.1$ ) make them potential candidates in the application of the internal heating control systems of lithium-ion batteries.

**Author Contributions:** Y.W.: investigation, data curation, methodology, writing—original draft preparation; X.C.: funding acquisition, writing—review and editing. All authors have read and agreed to the published version of the manuscript.

**Funding:** This research was funded by the National Natural Science Foundation of China under grant No. 51802204 and the Natural Science Foundation of Sichuan Province under Grant No. 2021YJ0523, China.

**Data Availability Statement:** Dataset available on request from the authors.

**Acknowledgments:** We appreciate Wang Hui from the Analytical and Testing Center of Sichuan University for her help with the SEM characterization.

**Conflicts of Interest:** The authors declare no conflicts of interest.

## References

1. Zhang, Y.; Fan, M.; Liu, X.; Huang, C.; Li, H. Beltlike  $\text{V}_2\text{O}_3@ \text{C}$  Core–Shell-Structured Composite: Design, Preparation, Characterization, Phase Transition, and Improvement of Electrochemical Properties of  $\text{V}_2\text{O}_3$ . *Eur. J. Inorg. Chem.* **2012**, *2012*, 1650–1659. [[CrossRef](#)]
2. Waldmann, T.; Wilka, M.; Kasper, M.; Fleischhammer, M.; Wohlfahrt-Mehrens, M. Temperature dependent ageing mechanisms in Lithium-ion batteries—A Post-Mortem study. *J. Power Sources* **2014**, *262*, 129–135. [[CrossRef](#)]
3. Wang, Y.; Zhang, X.; Chen, Z. Low temperature preheating techniques for Lithium-ion batteries: Recent advances and future challenges. *Appl. Energy* **2022**, *313*, 118832. [[CrossRef](#)]
4. Meng, S.; Dou, L.; Mu, M. Design of Thermal Management System for Lithium Battery at LOW Temperature. In Proceedings of the ITM Web of Conferences, Shanghai, China, 29–30 March 2022; EDP Sciences: Ulis, France, 2022; p. 03036.
5. Chen, P.; Lu, Z.; Ji, L.; Li, Y. Design of the control scheme of power battery low temperature charging heating based on the real vehicle applications. In Proceedings of the 2013 IEEE Vehicle Power and Propulsion Conference (VPPC), Beijing, China, 15–18 October 2013; IEEE: Piscataway, NJ, USA, 2013; pp. 1–6.
6. Al Hallaj, S.; Selman, J. A novel thermal management system for electric vehicle batteries using phase-change material. *J. Electrochem. Soc.* **2000**, *147*, 3231. [[CrossRef](#)]
7. Wang, P.-J.; Zeng, Z.-Q.; Gui, Z.-L.; Li, L.-T. Strontium-lead titanate ceramics with positive temperature coefficient of resistance. *Mater. Lett.* **1997**, *30*, 275–277. [[CrossRef](#)]
8. Kumar, M.; Garg, A.; Kumar, R.; Bhatnagar, M. Structural, dielectric and ferroelectric study of  $\text{Ba}_{0.9}\text{Sr}_{0.1}\text{Zr}_x\text{Ti}_{1-x}\text{O}_3$  ceramics prepared by the sol–gel method. *Phys. B Condens. Matter* **2008**, *403*, 1819–1823. [[CrossRef](#)]
9. Yu, A.; Li, Q.; Fan, D.; Zhang, H. Study on positive temperature coefficient of resistivity of co-doped  $\text{BaTiO}_3$  with Curie temperature in room temperature region. *Sci. China Technol. Sci.* **2019**, *62*, 811–819. [[CrossRef](#)]
10. Yu, L.; Xue, Q.; Zhang, R.; Tang, C.; Liu, S. On a sudden-changing PTC material with low curie temperature. *Electron Compon. Mater.* **1994**, *13*, 14–16. (In Chinese)
11. Patil, D.; Lokare, S.; Devan, R.; Chougule, S.; Kanamadi, C.; Kolekar, Y.; Chougule, B. Studies on electrical and dielectric properties of  $\text{Ba}_{1-x}\text{Sr}_x\text{TiO}_3$ . *Mater. Chem. Phys.* **2007**, *104*, 254–257. [[CrossRef](#)]
12. Hasegawa, A.; Fujitsu, S.; Yanagida, K.K. The enhanced penetration of oxygen along the grain boundary in semiconducting barium titanate. *Jpn. J. Appl. Phys.* **1991**, *30*, 1252. [[CrossRef](#)]
13. Alles, A.B.; Amarakoon, V.R.; Burdick, V.L. Positive temperature coefficient of resistivity effect in undoped, atmospherically reduced barium titanate. *J. Am. Ceram. Soc.* **1989**, *72*, 148–151. [[CrossRef](#)]
14. Alles, A.B.; Burdick, V.L. Grain boundary oxidation in PTCR barium titanate thermistors. *J. Am. Ceram. Soc.* **1993**, *76*, 401–408. [[CrossRef](#)]
15. Cheng, X.; Zhou, D.; Fu, Q.; Gong, S.; Qin, Y. Effect of reoxidation annealing on the PTCR behaviour of multilayer  $\text{Nb}^{5+}$ -doped  $\text{BaTiO}_3$  ceramics with a Ni internal electrode. *J. Phys. D Appl. Phys.* **2012**, *45*, 385306. [[CrossRef](#)]
16. Wang, X.; Chan, H.L.-W.; Choy, C.-I. Positive temperature coefficient of resistivity effect in niobium-doped barium titanate ceramics obtained at low sintering temperature. *J. Eur. Ceram. Soc.* **2004**, *24*, 1227–1231. [[CrossRef](#)]

17. Miki, T.; Fujimoto, A.; Jida, S. An evidence of trap activation for positive temperature coefficient of resistivity in BaTiO<sub>3</sub> ceramics with substitutional Nb and Mn as impurities. *J. Appl. Phys.* **1998**, *83*, 1592–1603. [[CrossRef](#)]
18. Gao, C.; Fu, Q.; Zhou, D.; Zu, H.; Chen, T.; Xue, F.; Hu, Y.; Zheng, Z.; Luo, W. Nanocrystalline semiconducting donor-doped BaTiO<sub>3</sub> ceramics for laminated PTC thermistor. *J. Eur. Ceram. Soc.* **2017**, *37*, 1523–1528. [[CrossRef](#)]
19. Lin, T.-F.; Hu, C.-T.; Lin, I.-N. Defects restoration during cooling and annealing in PTC type barium titanate ceramics. *J. Mater. Sci.* **1990**, *25*, 3029–3033. [[CrossRef](#)]
20. Kolodiazny, T.; Tachibana, M.; Kawaji, H.; Hwang, J.; Takayama-Muromachi, E. Persistence of ferroelectricity in BaTiO<sub>3</sub> through the insulator-metal transition. *Phys. Rev. Lett.* **2010**, *104*, 147602. [[CrossRef](#)] [[PubMed](#)]
21. Liu, J.; Gong, S.; Quan, L.; Chen, B.; Zhou, D. Reoxidation effects of Ba-excessive barium titanate ceramics for laminated positive temperature coefficient thermistors. *J. Am. Ceram. Soc.* **2012**, *95*, 1640–1644. [[CrossRef](#)]
22. Heywang, W. Resistivity anomaly in doped barium titanate. *J. Am. Ceram. Soc.* **1964**, *47*, 484–490. [[CrossRef](#)]
23. Jonker, G. Some aspects of semiconducting barium titanate. *Solid-State Electron.* **1964**, *7*, 895–903. [[CrossRef](#)]
24. Hendrix, B.; Wang, X.; Chen, W.; Cui, W. Understanding doped V<sub>2</sub>O<sub>3</sub> as a functional positive temperature coefficient material. *J. Mater. Sci. Mater. Electron.* **1992**, *3*, 113–119. [[CrossRef](#)]
25. Yan, F.; Han, W.; Wang, X.; Chen, J.; Wei, L. The effect of Cr dopant concentration on electrical property of (V<sub>1-x</sub>Cr<sub>x</sub>)<sub>2</sub>O<sub>3</sub> nano-grain ceramics. *Mater. Res. Bull.* **2013**, *48*, 2365–2369. [[CrossRef](#)]

**Disclaimer/Publisher's Note:** The statements, opinions and data contained in all publications are solely those of the individual author(s) and contributor(s) and not of MDPI and/or the editor(s). MDPI and/or the editor(s) disclaim responsibility for any injury to people or property resulting from any ideas, methods, instructions or products referred to in the content.